Journal of Luminescence 213 (2019) 334–342

Contents lists available at ScienceDirect

Journal of Luminescence

journal homepage: www.elsevier.com/locate/jlumin

Comprehensive analysis of thermoluminescence signals in MgB_4O_7:Dy,Na dosimeter

Vasilis Pagonis[a,*], Nathan Brown[b], George S. Polymeris[c], George Kitis[d]

[a] Physics Department, McDaniel College, Westminster, MD, 21157, USA
[b] Department of Earth and Planetary Sciences, University of California, Berkeley, CA, 94720, USA
[c] Institute of Nuclear Sciences, Ankara University, Beşevler, 06100, Ankara, Turkey
[d] Aristotle University of Thessaloniki, Nuclear Physics Laboratory, 54124, Thessaloniki, Greece

ARTICLE INFO

Keywords:
Magnesium borate
MgB_4O_7:Dy,Na
Tunneling model
TL temperature sensing

ABSTRACT

Magnesium borate (MgB_4O_7) is a material of interest for thermoluminescence (TL) dosimetry of ionizing radiation, due to its low photon energy dependence and the possibility of developing neutron dosimeters, and its potential as a temperature sensor in passive temperature sensing applications. Recent experimental and modeling work has shown that TL glow curves and isothermal luminescence signals in MgB_4O_7:Dy,Na can be analyzed using a radiative tunneling model, based on localized recombination processes. This paper presents a comprehensive analysis of TL signals in MgB_4O_7:Dy,Na dosimeters, based on a recently published model which incorporates simultaneous irradiation and tunneling processes. Four different types of TL data are presented and analyzed using the proposed model: (a) TL glow curves at different irradiation doses, (b) TL signals after sample irradiation at different temperatures, (c) TL after isothermal heating for 500 s at various temperatures, and (d) TL after room temperature irradiation, followed by heating to a temperature T_{stop}. We also present an alternative fast and efficient Monte Carlo method of analyzing the data, which is very useful for quick analysis of experimental data. The experimental data and modeling results show that the shape of the TL glow peaks remains essentially the same in all four experimental protocols, while the height and temperature of maximum TL intensity depends on the irradiation and preheating conditions.

1. Introduction

Magnesium borate (MgB_4O_7) doped with rare earth elements is a material of interest in thermoluminescence (TL) dosimetry of ionizing radiation ([1–7]). Some of the properties which make MgB_4O_7 attractive as a TL dosimeter is its low effective atomic number, low photon energy dependence, and the possibility of developing neutron dosimeters based on its high neutron capture cross-section ([1,3,8]). There has also been extensive recent interest in this material, as a possible passive temperature sensor ([9–12]). A few systematic studies have been carried out on the TL of MgB_4O_7 doped with a variety of rare earth elements, and showed that different dopants were associated with TL peaks at different temperatures, and with different trapping mechanisms ([9,12]).

In a recent extensive experimental and modeling study, Kitis et al. [13] investigated and compared prompt isothermal decay (PID) of TL signals in MgB_4O_7:Dy,Na and LiB_4O_7:Cu,In dosimeters, in order to elucidate the luminescence mechanism in these two materials. These authors showed that PID signals in MgB_4O_7:Dy,Na were consistent with a localized radiative tunneling mechanism, while signals in LiB_4O_7:Cu,In were likely to be produced by a delocalized radiative recombination mechanism involving the conduction band.

In this paper, we extend the work of Kitis et al. [13], to TL signals measured during four different types of experiments. Specifically the 4 types of TL signals are: (a) TL glow curves at different irradiation doses, (b) TL signals after sample irradiation at different temperatures, (c) TL after isothermal heating at various temperatures, and (d) TL after room temperature irradiation, followed by heating to a temperature T_{STOP}.

The experimental data are analyzed using two models. Firstly, a *qualitative* modeling study is carried out based on the work of Brown et al. [14], which includes simulated multistage processes of irradiation, heating and quantum tunneling. Secondly, a *quantitative* modeling study is carried out based on the recently published simpler Monte Carlo method of Pagonis et al. [15]. An important result from both the experimental data and the modeling results is that the *shape* of the TL glow peaks does not change significantly with the preheating

* Corresponding author.
E-mail address: vpagonis@mcdaniel.edu (V. Pagonis).

https://doi.org/10.1016/j.jlumin.2019.05.044
Received 1 April 2019; Received in revised form 17 May 2019; Accepted 17 May 2019
Available online 20 May 2019

conditions.

The specific goals of the paper are:

(a) To investigate experimentally the variation of the TL glow curves with irradiation dose, irradiation temperature, preheating temperature and isothermal preheating conditions.
(b) To provide a qualitative description of the experimental data, by adopting the tunneling model developed by Brown et al. [14] for feldspars.
(c) To provide a *quantitative* description of the experimental data, by using the simpler Monte Carlo method of Pagonis et al. [15].
(d) To discuss possible implications of the experimental and simulation results for thermochronology applications.

2. Experimental

This section describes the four types of TL experiments carried out in MgB_4O_7:Dy,Na. The experimental data from Experiments #1 and #2 which are described in detail below, have been previously published by Furetta et al. [16] and Kitis et al. [13], correspondingly. Experiments #3 and #4 concern new unpublished data.

2.1. Experiment #1: prompt TL measurements at different irradiation doses

Furetta et al. [16] presented an extensive study of the dosimetric properties of MgB_4O_7:Dy,Na detectors. Some of their experimental data are reproduced in Fig. 1a. This experimental data was obtained using a Model 2000 TL Analyser manufactured by the Harshaw Chemical Co., with a heating rate of 5°C/s. The dosimeters were exposed to ^{60}Co gamma radiation and the TL measurements were carried out on solid sintered pellets of 4.6 mm in diameter and 0.95 mm in thickness. The dosimeters were protected from direct light during handling, irradiation and read-out procedures. There was no significant time delay between the irradiation and read-out of the samples.

It is noted that the experimental data in Fig. 1 shows a single TL peak at ~190°C. The TL glow curves from other batches of this dosimetric material contain additional smaller peaks at either lower and/or higher temperatures. For example, the TL glow curves shown in Figs. 2–4 of this paper are from a different batch of this material, and they contain an additional smaller peak at 350°C.

2.2. Experiment #2: Remnant-TL (RTL) measurements, after irradiation and isothermal decay for 500 s at various constant temperatures

Kitis et al. [13] studied prompt isothermal decay signals from MgB_4O_7:Dy,Na detectors. A subset of their experimental RTL glow curves is shown in Fig. 2, for T_{ISO} = 88-193°C, in steps of 7°C.

The experimental protocol of Kitis et al. [13] was as follows:

Step 0: Dose of 1 Gy, and TL measurement up to 450°C, to clear the traps.

Step 1: The same aliquot is irradiated with a dose of 1 Gy, in order to populate the traps.

Step 2: TL measurement up to a temperature T_{ISO} at 2°C/s. The sample is held for 500 s at this temperature, and the corresponding isothermal decay signal is measured.

Step 3: After the end of the decay period, the sample is cooled down to room temperature.

Step 4: TL measurement at 2°C/s in order to obtain the remnant-TL glow curve (RTL).

Step 5: Repeat steps 1–4 for a new decay temperature T_{ISO}.

The RTL measurements shown in Fig. 2 were carried out using a Risø TL/OSL reader (model TL/OSL-DA-15), equipped with a ^{90}Sr/^{90}Y beta particle source, delivering a nominal dose rate of 0.105 Gy/s. A 9635QA photomultiplier tube with a combination of Pilkington HA-3 heat absorbing and a Corning 7–59 blue filter (320-440 nm) were used for light detection. All measurements were performed in a nitrogen

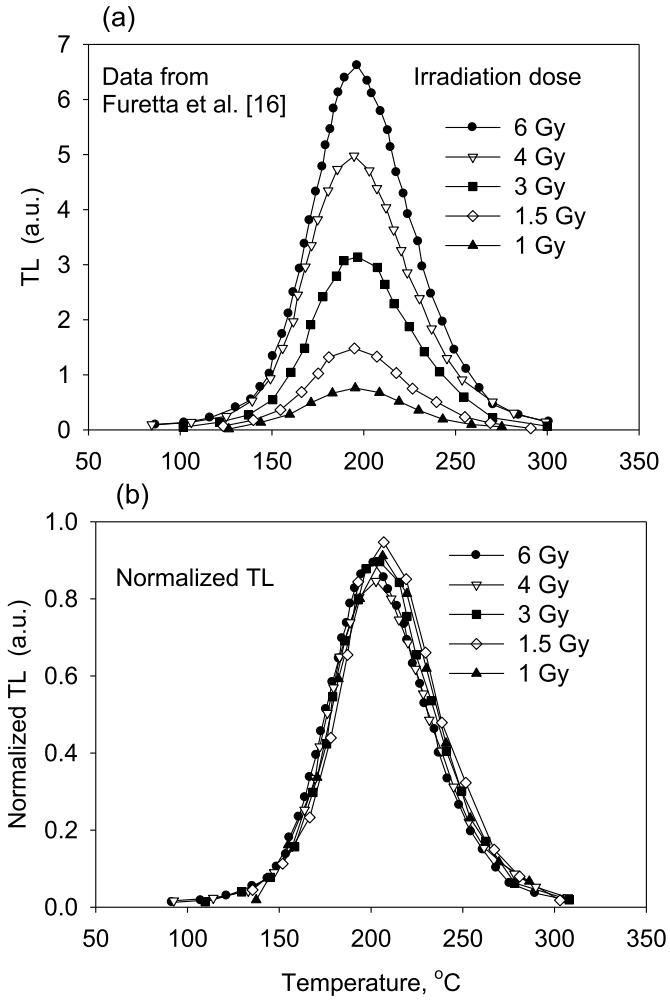

Fig. 1. Experimental data from Furetta et al. [16]. (a) The prompt TL glow curves for a sample irradiated at 5 different doses in the range 1-6 Gy (b) The same experimental data as in (a), with the TL glow peaks normalized along the y-axis, showing that the irradiation dose does not change significantly the shape and width of the glow curve.

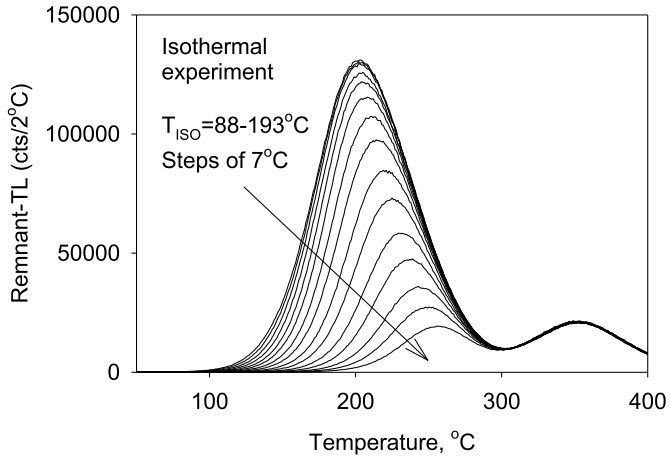

Fig. 2. The remnant-TL (RTL) glow curves from the prompt isothermal decay experiment by Kitis et al. [13]. Irradiation takes place at room temperature, followed by isothermal heating for 500 s at a temperature T_{ISO}, followed by measurement of RTL glow curves. The experimental RTL glow curves were measured for T_{ISO} = 88-193°C, in steps of 7°C. The direction of the arrow shows increasing values of T_{ISO}.

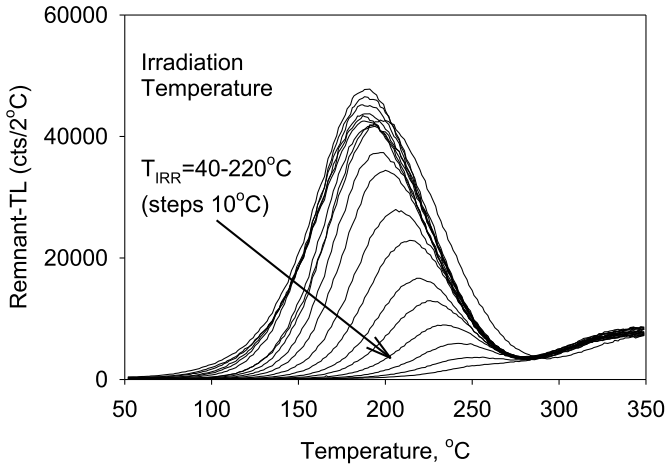

Fig. 3. RTL curves obtained by irradiating the sample at different irradiation temperatures T_{IRR} = 40-220°C, in steps of 10°C. The trend is very similar to the behavior seen in Fig. 2, and the direction of the arrow shows increasing values of T_{IRR}.

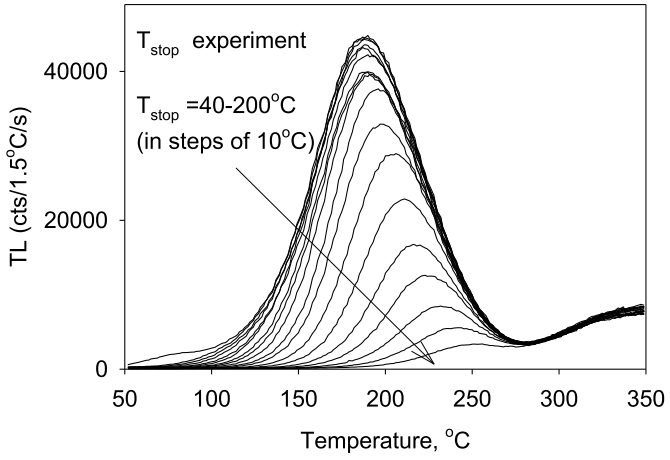

Fig. 4. RTL curves obtained by irradiating the sample at room temperature, then heating up to a temperature T_{STOP}, followed by measurement of RTL up to 450°C with a heating rate of 2°C/s. The temperatures T_{STOP} = 40-200°C, in steps of 10°C.

atmosphere with a low constant heating rate of 2°C/s, and the samples were heated up to the maximum temperature of 450°C.

2.3. Experiment #3: RTL after irradiation at elevated temperatures T_{IRR}

The protocol for this new type of experiment was as follows:

Step 1: Heat the sample up to preselected irradiation temperature (T_{IRR}), with a heating rate of 2° C/sec. Leave the sample at this temperature for 1 min, in order to attain the required T_{IRR}

Step 2: Irradiate the sample at T_{IRR}, with a dose of 0.15 Gy. This is the crucial step, where irradiation takes place at an elevated temperature.

Step 3: Immediately after the end of irradiation, the heating is stopped and the sample is cooled to room temperature.

Step 4: TL measurement at 2°C/s in order to obtain the remnant-TL glow curve (RTL).

The experimental RTL glow curves from this third type of experiment are shown in Fig. 3, for irradiation temperatures T_{IRR} = 40-220°C, in steps of 10°C.

2.4. Experiment #4: RTL after irradiation and partial heating to elevated temperatures T_{STOP}

The experimental protocol for this new type of experiment was as follows:

Step 1: Irradiate sample with a dose of 0.15 Gy.

Step 2: Heat the sample up to a temperature T_{STOP}, with a heating rate of 2°C/sec.

The heating is stopped and the sample is cooled to room temperature.

Step 3: RTL measurement up to 450°C with a heating rate of 2°C/s.

Step 4: Repeat the sequence for a new temperature T_{STOP} in Step 2.

The experimental RTL glow curves from this fourth type of experiment are shown in Fig. 4, for temperatures T_{STOP} = 40-200°C, in steps of 10°C.

3. Experimental results

3.1. Experiment #1: prompt TL measurements at different irradiation doses

In the experimental data of Fig. 1a, the sample is irradiated with 5 different doses in the range 1-6 Gy and the prompt TL signal is measured immediately after. As the dose is increased, the temperature of maximum TL intensity does not change, and the maximum TL intensity is proportional to the irradiation dose. Fig. 1b shows the same experimental data as Fig. 1a, with the TL glow peaks normalized along the y-axis. The results of Fig. 1b show that the normalized TL glow peaks coincide almost completely, indicating that the irradiation dose does not change significantly the shape or the width of the glow peak.

Furetta et al. [17] analyzed the main dosimetric peak in this material by using the empirical general order kinetics. They found that both the activation energy *E* and the kinetic order *b* increased with the storage time after irradiation. They concluded that the TL emission is due to a quasi-continuous trap distribution. The recent detailed study of Kitis et al. [13] confirmed this quasi-continuous distribution of energies, and established that the TL glow peaks can be described within the tunneling model of Jain et al. [18]. The physical assumptions of this model are the presence of a random distribution of defects in the material, and that luminescent recombination takes place via localized transitions, instead of proceeding by delocalized transitions involving the energy bands.

3.2. Experiment #2: RTL measurements, after irradiation and isothermal decay for 500 s at variable constant temperatures

Fig. 2 shows the experimental RTL glow curves obtained after isothermal decay of the TL signal for 500 s, and for different temperatures T_{ISO} = 88-193°C, in steps of 7°C. As the isothermal temperature is increased in the direction of the arrow, the height of the TL glow peak decreases, and the temperature of maximum TL intensity shifts towards higher temperatures.

This behavior is exactly similar to that reported by Pagonis et al. [19] and Sfampa et al. [20] for feldspars, which are materials exhibiting the anomalous fading effect due to quantum tunneling processes. Furthermore, such a behavior is predicted by the localized tunneling recombination model by Jain et al. [18].

3.3. Experiment #3: RTL after irradiation at elevated temperatures T_{IRR}

Fig. 3 shows the experimental RTL glow curves measured for irradiation temperatures T_{IRR} = 40-220°C, in steps of 10°C. The trend is very similar to the behavior seen in Fig. 2; as the irradiation temperature increases in the direction of the arrow, the TL glow peaks decrease in height and shift towards higher temperatures, while the high temperature part of the TL glow curve remains unaffected.

To the best of our knowledge, this is the first experimental report of

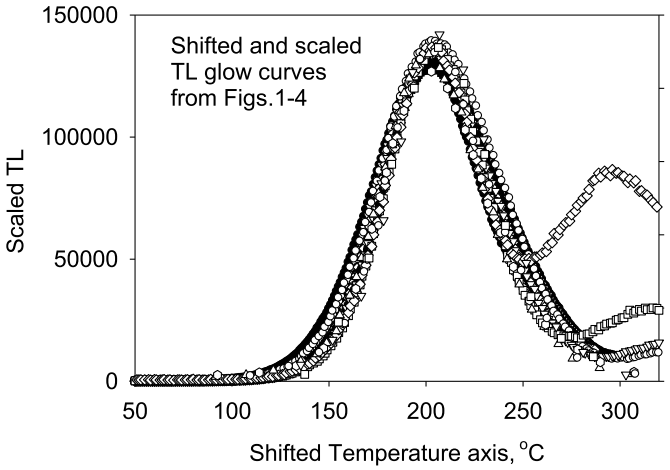

Fig. 5. Selected experimental data from Figs. 1–4; the TL glow peaks are shifted along the temperature axis, and also normalized along the y-axis. The resulting 16 shifted/scaled TL glow peaks practically coincide within experimental error, indicating that the shape/width of the TL glow peaks remains essentially unchanged under the experimental conditions in the 4 experiments.

the behavior of TL signals in this material as a function of the irradiation temperature.

3.4. Experiment #4: RTL after irradiation and partial heating to elevated temperatures T_{STOP}

The experimental RTL glow curves from this fourth type of experiment are shown in Fig. 4, for temperatures T_{STOP} = 40-200°C, in steps of 10°C. This set of data is very similar to the experimental data from a microcline sample, reported by Pagonis et al. [19].

Before attempting to analyze the experimental data in Experiments #1-#4 in a detailed manner, we selected 4 TL glow curves from each of Figs. 1–4, and examined the shape of the TL glow curves by shifting them along the temperature axis, and also normalizing them along the y-axis. The result of this shifting and normalizing procedure for the 16 TL glow curves is shown in Fig. 5. The TL glow peaks practically coincide within experimental error, indicating that the width of the TL glow peak remains essentially unchanged under the experimental conditions in the 4 experiments. The margins of error in the FWHM of the glow peaks shown in Fig. 5 can be estimated by fitting with a symmetric Gaussian curve on an empirical basis. The results of such a fit are FWHM = (68 ± 5) K (1σ). This practically unchanging shape of the TL glow peaks is discussed further in Sections 4 and 5, and a theoretical explanation was presented recently elsewhere (Pagonis and Brown [21]).

In the next two sections of this paper, the experimental data in Figs. 1–4 are analyzed using two different approaches. Section 4 presents *qualitative* simulations based on the work by Brown et al. [14] in feldspars. While this type modeling work can be used to describe the TL data in a quantitative manner as well, it is not suitable for quick analysis of the experimental data, since it requires several consecutive numerical integrations. Therefore, in Section 5 we present an additional simpler *quantitative* analysis of the experiments, based on the Monte Carlo method recently suggested by Pagonis et al. [15] for feldspar samples.

4. The model by Brown et al. [14] -Comparison with experiment

Brown et al. [14] investigated the simultaneous effects of irradiation and quantum tunneling on the TL glow curves in materials within a random distribution of defects. These authors extended the original model by Jain et al. [18], to include irradiation processes. Fig. 6 shows a schematic diagram of the model in [14], indicating the various processes which are involved during natural or laboratory irradiation of a feldspar sample. Process (i) represents the sample irradiation process, which can take place in one of two different ways: either in nature with a very slow natural dose rate of the order of 1 Gy/Ka, or in the laboratory with much higher dose rates of the order of 0.1 Gy/s.

Process (ii) in Fig. 6 represents thermal excitation of electrons from the ground into the excited state of the trapped electron, followed by either de-excitation into the ground state possibly by phonon emission (process iii), or by tunneling into the recombination center shown as (iv) in Fig. 6. The model implicitly assumes that electrons transportation to the band tail states and also to the conduction band is a much smaller effect than the effect of the excited state.

Brown et al. [14] investigated the simultaneous effects of irradiation and tunneling by using the differential equation:

$$\frac{\partial n(r',t)}{\partial t} = \frac{\dot{D}}{D_o}[N(r') - n(r',t)] - n(r',t)\exp[-\Delta E/k_B T]\frac{P(r')s}{P(r')+s} \quad (1)$$

where $n(r',t)$ (m^{-3}) is the instantaneous concentration of trapped electrons in the ground state; this concentration depends on both the elapsed irradiation time t and on the dimensionless distance parameter $r' = (4\pi\rho/3)^{1/3}r$, where r (m) is the separation distance r between donor and acceptor, and ρ (m^{-3}) represents the actual density of recombination centers in the material. Similarly, one introduces the dimensionless density parameter ρ' of recombination centers, as $\rho' = (4\pi\rho/3)a^3$, where a (m) is the potential barrier tunneling length (Jain et al. [18]). The parameter T represents the temperature of the sample, k_B is the Boltzmann constant, s (s^{-1}) is the trap frequency factor and ΔE (eV) is the thermal activation energy of the trap from the ground state to the excited state. $N(r')(m^{-3})$ is the total concentration of trapped electrons corresponding to a distance parameter r', $\dot{D}$(Gy/s) is the irradiation rate and D_o (Gy) is the characteristic dose of the material.

The total concentration of trapped electrons $N(r')$ corresponding to a distance r' is given by the well known nearest neighbor distribution:

$$N(r') = N\{3(r')^2\exp[-(r')^3]\} \quad (2)$$

where N (m^{-3}) is the total concentration of traps in the material. The excited-state tunneling probability $P(r')$ in Eqt.(1) decreases with r' according to:

$$P(r') = P_o\exp[-(\rho')^{-1/3}r'] \quad (3)$$

where P_o (s^{-1}) is the frequency characterizing the tunneling process.

The term $\frac{\dot{D}}{D_o}[N(r') - n(r',t)]$ in Eqt.(1) represents the rate of increase of the concentration $n(r',t)$ due to irradiation, while the second term $n(r',t)\exp[-\Delta E/k_B T]\frac{P(r')s}{P(r')+s}$ in Eqt.(1) represents the decrease in the concentration $n(r',t)$ due to the combined effect of tunneling and thermal excitation processes. These equations are valid for samples irradiated in nature with a very slow dose rate $\dot{D}$(Gy/s), but also for samples irradiated with much higher dose rates in the laboratory.

Equation (1) can be solved numerically to simulate the multistage Experiments #1-#4, with the *final* concentrations of $n(r',t)$ at the end of each stage, being used as the *initial* concentrations for the *next* stage in the simulations.

In order to simulate the TL glow curves in Experiments #1-#4, Eqt. (1) must be solved with a constant heating rate β (K/s), and the time-dependent TL intensity $L(t)$ is evaluated numerically by integrating the rate of change of the concentration $\partial n(r',t)/\partial t$ over all possible values of the variable r' [15]:

$$L(t) = -\int_0^\infty \frac{\partial n(r',t)}{\partial t}dr'. \quad (4)$$

In Experiment #1, the prompt TL glow curve is measured immediately after the irradiation process in the laboratory. Therefore, simulation of Experiments #1 involves only two stages:

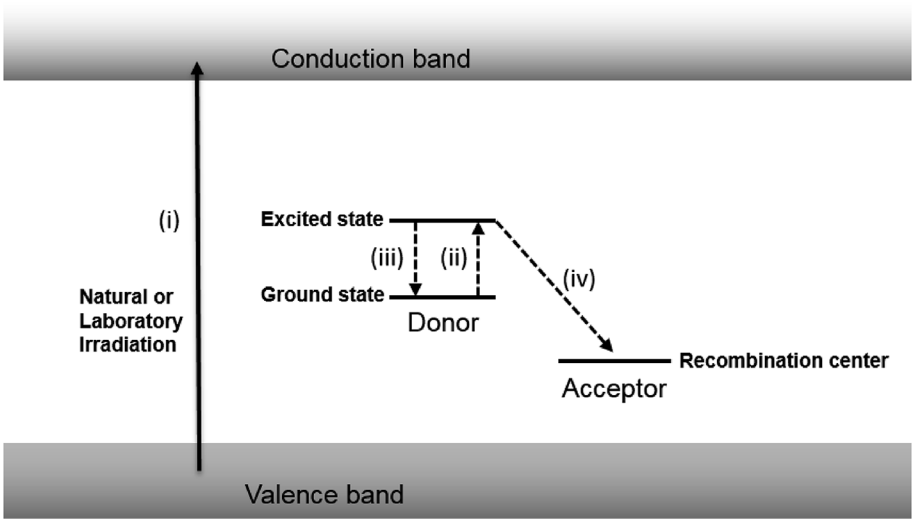

Fig. 6. Schematic diagram of the model by Brown et al. [14], showing the various processes assumed involved during natural or laboratory irradiation of a feldspar sample. Process (i) represents the sample irradiation process, either in nature with a slow natural dose rate of the order of 1 Gy/Ka, or in the laboratory with much higher dose rates of the order of 0.1 Gy/s. Process (ii) represents thermal excitation of electrons from the ground into the excited state of the trapped electron, followed by either de-excitation into the ground state (process iii), or by tunneling into the recombination center shown as (process iv), depending on which transition is more probable given the distance between donor and acceptor.

(a) Irradiation stage: integrate equation (1) for a certain irradiation time t_{IRR} to obtain the concentration $n(r', t_{IRR})$ at the end of the irradiation process, and
(b) TL stage: integrate equation (1) with a constant heating rate using concentration $n(r', t_{IRR})$ as the initial conditions, then integrate equation (4) to obtain the TL glow curve.

In Experiment #2, the simulation involves these four stages:

(a) Irradiation stage, as above
(b) Heating stage to temperature T_{ISO}: integrate equation (1) with a constant heating rate of 2°C/s, using concentration $n(r', t_{IRR})$ as the initial conditions.
(c) Isothermal stage: integrate equation (1) for a total time of 500 s at a constant temperature T_{ISO}.
(d) TL stage, as above.

In Experiment #3, the simulation involves these two stages:

(a) Irradiation stage, at a constant irradiation temperature T_{IRR}.
(b) TL stage, as above.

In Experiment #4, the simulation involves these three stages:

(a) Irradiation stage, as above
(b) Heating stage to temperature T_{STOP}: integrate equation (1) with a constant heating rate of 2°C/s, using concentration $n(r', t_{IRR})$ as the initial conditions.
(c) TL stage, as above.

Examples of this rather complex type of numerical analysis were given previously in Polymeris et al. [22]. These authors provided a quantitative analysis of the TL glow peaks for feldspar samples that were preheated at various elevated temperatures, and for various preheating times.

The results of simulating Experiments #1-#4 are shown in Fig. 7a–d, for samples irradiated with a high dose rate in the laboratory. The parameters used in all these simulations are $\rho' = 0.01$, $\Delta E = 1.02$ eV, $s = 2x10^{11}$ s^{-1}, $\beta = 2$ K/s, laboratory dose rate $\dot{D}$=0.1 Gy/s, characteristic dose D_o = 1600 Gy.

Fig. 7e is a different type of simulation, showing the simulated TL glow peaks for a sample irradiated *in nature* and for different time intervals in the range $t_{IRR} = 10^2$-10^5 y. These simulations are carried out with a very slow natural dose rate of $\dot{D}$=2.85 Gy/Ka, and the irradiation temperature was T_{IRR} = 20 °C. Fig. 7e shows that as the irradiation time is increased, the RTL glow peaks increase gradually to saturation, and shift towards higher temperatures. From a physical point of view, this means that for long irradiation times more proximal electron-hole pairs have recombined, and that the average distance between pairs gets larger. Saturation of the RTL signal is clearly seen at high irradiation times of $\sim 10^6$ y. The elapsed time until saturation will depend on the ratio $D_o/\dot{D}$.

Fig. 7f shows the results of shifting the 20 TL glow peaks from Fig. 7a–e along the x-axis, and also scaling them along the y-axis. When the TL glow peaks in Fig. 7a–e are shifted and scaled in this manner, they become practically identical, showing that the shape of the TL glow peaks remains essentially unchanged.

The results of Fig. 7 demonstrate that the experimental results in Figs. 1–4 can be described by using the multistage simulation method by Brown et al. [14]. However, this multistage simulation method is rather cumbersome and tedious, requiring several consecutive numerical integrations. In the next section we provide an alternative method of analyzing the experimental data, by using a recently published efficient Monte Carlo method [15].

5. 4. The Monte Carlo method of Pagonis et al. [15] -comparison with experiment

The sequence of TL glow peaks in Figs. 1–4 can be described quantitatively by using a Monte Carlo (MC) method recently described in Pagonis et al. [15], their equation (11). The MC method evaluates the total concentration of remaining electrons and the luminescence intensity simultaneously, by using the following difference equations for the discrete variable $n(r',t)$ in the general form:

$$\Delta n(r', t) = -\frac{(A s_{tun}/B)}{\exp[(\rho')^{-1/3} r']} n(r', t)\Delta t = -\frac{(s_{th} s_{tun}/B)\exp[-\Delta E/(k_B T)]}{\exp[(\rho')^{-1/3} r']} n(r', t)\Delta t \quad (5)$$

$$n(t) = \sum_{r'=0}^{2} n(r', t)\ \Delta r' \quad (6)$$

$$L(t) = -\sum_{r'=0}^{2} \frac{\Delta n(r', t)}{\Delta t}\ \Delta r' \quad (7)$$

The various symbols in these equations are defined as follows. $n(r', t)$ is the instantaneous concentration of remaining trapped electrons in the system, and is a function of time t (s) and of the dimensionless distance parameter $r' = (4\pi\rho/3)^{1/3} r$, where ρ (m^{-3}) represents the actual density of recombination centers in the material and

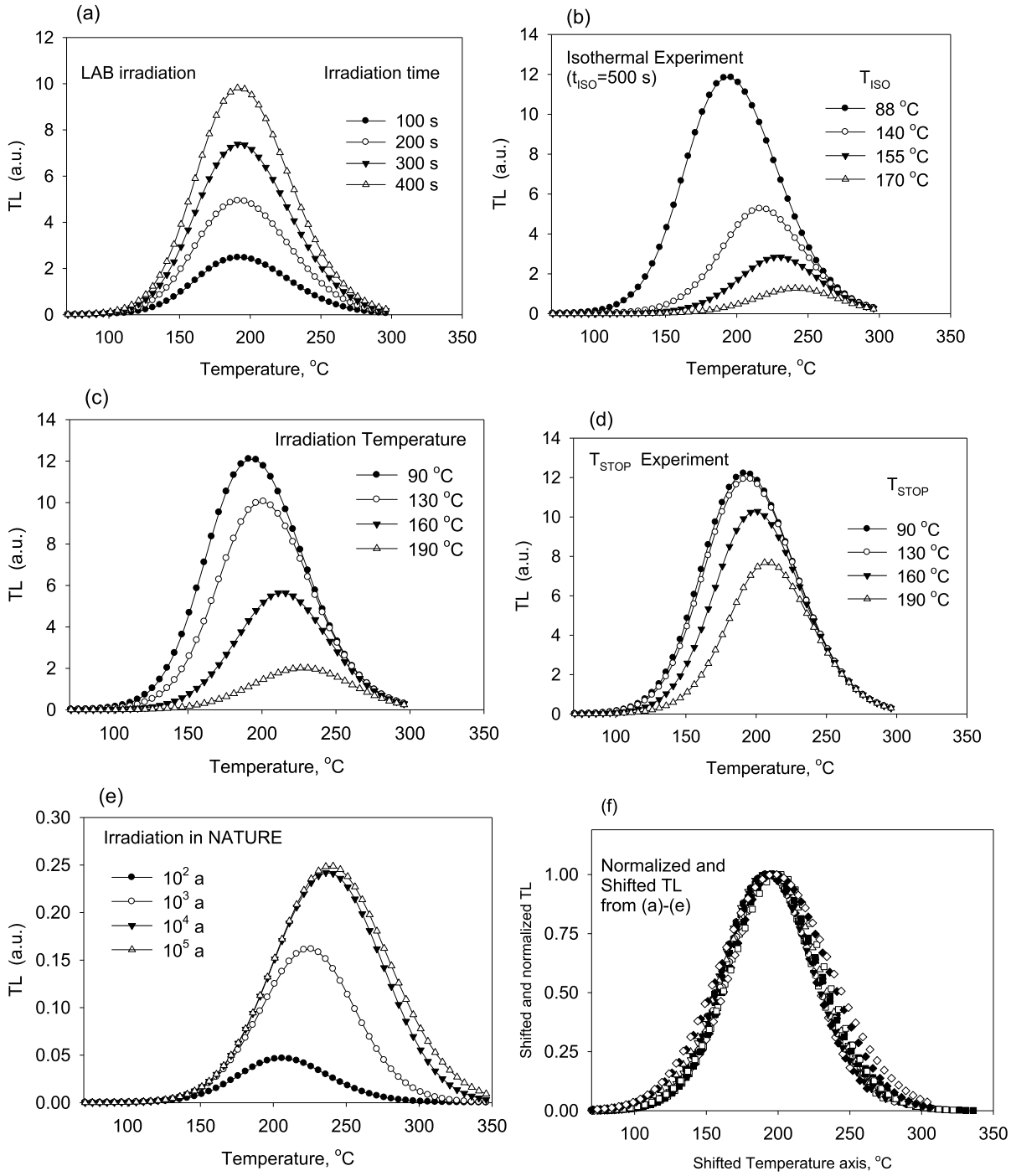

Fig. 7. (a) – (d) The results of simulating Experiments #1-#4, for samples irradiated with a high dose rate in the laboratory. The parameters used in all these simulations are $\rho' = 0.01$, $\Delta E = 1.02$ eV, $s = 2x10^{11}$ s^{-1}, $\beta = 2$ K/s, laboratory dose rate $\dot{D}$=0.1 Gy/s, characteristic dose D_o = 1600 Gy. (e) The simulated TL glow peaks for a sample irradiated *in nature* and for different time intervals $t_{IRR} = 10^2$-10^5 y, with a slow natural dose rate of$\dot{D}$=2.85 Gy/ka, and at an irradiation temperature T_{IRR} = 20 °C. (f) The results of shifting the 20 TL glow peaks from Fig. 7a–e along the x-axis, and also scaling them along the y-axis. The shifted-scaled TL glow peaks are practically identical, showing that the shape and width of the TL glow peaks in (a)-(e) stays practically the same.

r (m) is the distance between donors and acceptor pairs. Similarly, one introduces the dimensionless density of recombination centers $\rho' = (4\pi\rho/3)\alpha^{-3}$, where α (m^{-1}) is the potential barrier penetration constant (Jain et al., [18]).

In the above equations s_{tun} (s^{-1}) is the frequency factor characterizing the tunneling process taking place from the excited state of the system (transition iv, Fig. 6). $A = s_{th} \exp(-E/k_B T)$ (s^{-1}) is the thermal excitation rate from the ground to the excited state (transition ii, Fig. 6), where E (eV) is the thermal activation energy and s_{th} (s^{-1}) is the pre-exponential factor for the thermal excitation process, which is proportional to the lattice vibration frequency. B (s^{-1}) is the rate of de-excitation from the excited state back to the ground state (transition iii, Fig. 6). From a physical point of view, there is no relationship between the three different frequency factors s_{th}, B and s_{tun}. In a TL experiment, the sample is heated with a linear heating rate β ($K{\cdot}s^{-1}$), from a starting temperature T_o up to a high temperature around 500 °C, so that the temperature varies as $T(t) = T_o + \beta t$. Furthermore, it is noted that the three frequency factors s_{th}, B and s_{tun} do not appear as separate

quantities in Eqt.6, but rather as the combination $s_{th}s_{tun}/B$, which defines an "effective frequency factor" $A_{TL} = s_{th}s_{tun}/B$ for the TL process. Therefore Eqt.5 can be written in the simplified form:

$$\Delta n(r',\, t) = -\frac{A_{TL}\exp[-\Delta E/(k_B T)]}{\exp[(\rho')^{-1/3}r']} n(r',\, t)\Delta t \tag{8}$$

In the Monte Carlo procedure $\Delta r'$ is an appropriate distance interval, e.g. $\Delta r' = 0.02$, and Δt is an appropriate time interval, e.g. $\Delta t = 1\ s$. As was discussed in Pagonis et al. ([15]), software implementation proceeds by following the evolution of the system for *both* the time variable t, and for each value of the dimensionless distance r'. The rate P for an electron to recombine radiatively within the time interval Δt and for certain distance r' is given by the function $A_{TL}\exp[-\Delta E/(k_B T)]/\exp[(\rho')^{-1/3}r']$ in the right hand side of equation (7). One chooses a suitable value of Δt so that $P\Delta t << 1$, and a random number r is generated, which is uniformly distributed in the unit interval $0 \le r < 1$. If $r \le P$ the electron recombines radiatively, otherwise it does not; the contributions from all distances r' are added according to Eqts. (6) and (7), resulting in the simultaneous evaluation of the discrete-value functions $n(t)$ and $L(t)$. The MC simulations reach a precision of 1 % rather quickly, by repeating N = 10–20 cycles of 200 electrons each.

Although the above Eqns. (5)–(8) were strictly derived *for freshly irradiated samples*, Pagonis et al. [15] demonstrated how they can also be used for samples which were exposed to optical and thermal pretreatments. Examples of such combined treatments are an IR bleaching followed by TL measurement, an IR treatment followed by isothermal decay, a partial heating followed by TL measurement etc. For such pretreated samples, one can approximate the nearest neighbor distribution with a *truncated* distribution function, which extends from a minimum critical radius r'_c up to infinity ([15]). This critical radius can be treated as an adjustable modeling parameter when fitting experimental data. For such truncated distributions, the summations in Eqts. (6) and (7) will extend from a minimum critical radius r'_c, instead of starting at $r'_c = 0$ ([15]).

The results of using this MC technique are shown in Figs. 8–11, where they are compared with the results from Experiments #1-#4 respectively. The agreement between the Monte Carlo model and the four sets of experimental data is very good, indicating that the model provides a satisfactory *quantitative* description of the luminescence

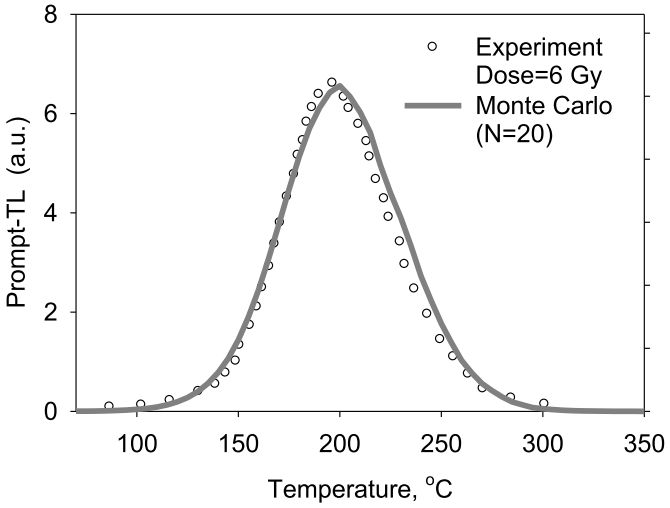

Fig. 8. The solid lines represent Monte Carlo simulations of Experiment #1, and are compared with selected experimental data from Fig. 1. The MC simulations were carried out using the method of Pagonis et al. [15], and Eqts.(5)-(7). The model parameters are $E = 1.01$ eV, $A_{TL} = 2 \times 10^{11}\ s^{-1}$ and $\rho' = 0.019$. The value of the critical distance in these simulations was $r'_c = 0$, since the samples were not treated thermally after irradiation.

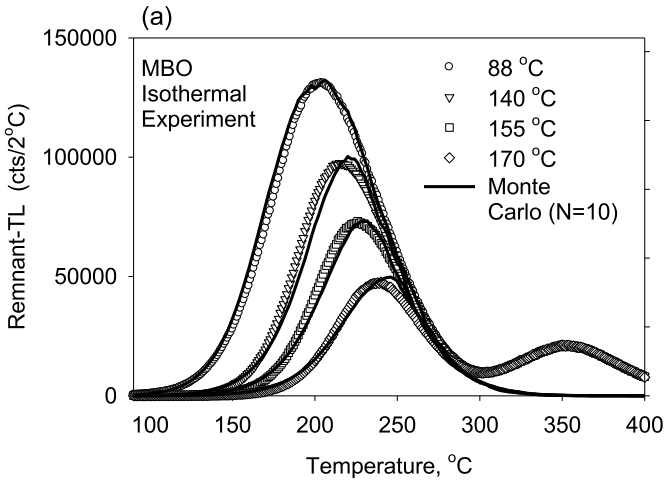

Fig. 9. The solid lines represent Monte Carlo simulations of Experiment #2 (RTL after isothermal heating), and are compared with selected experimental data from Fig. 2. MC was carried out with the slightly modified set of parameters $E = 1.02$ eV, $A_{TL} = 2 \times 10^{11}\ s^{-1}$ and $\rho' = 0.01$. The value of the critical distance for the 4 RTL graphs shown here are $r'_c = 0,\ 0.8,\ 0.95,\ 1.1$.

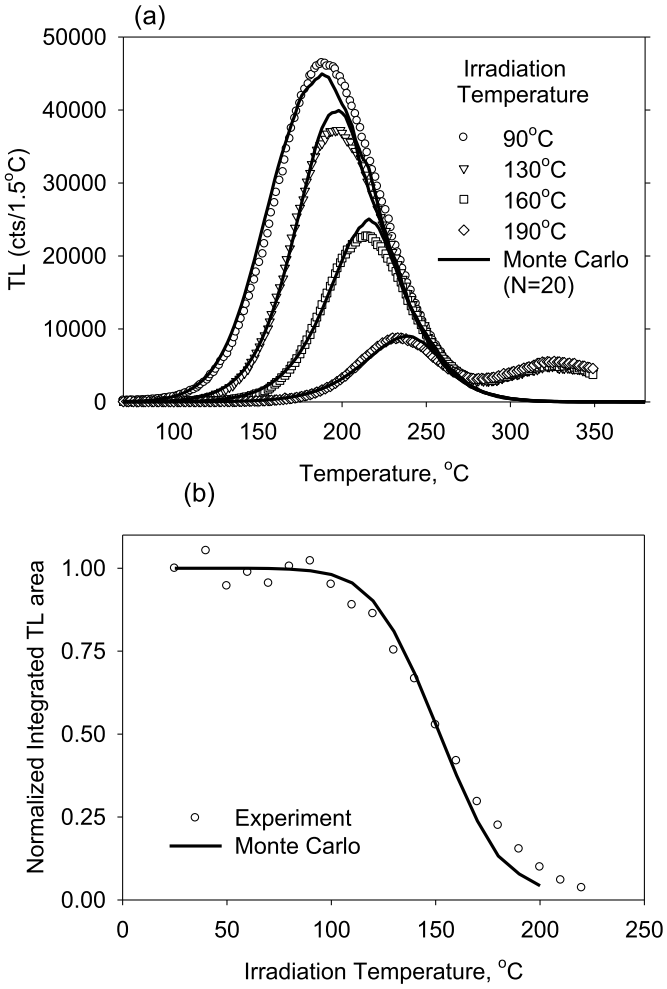

Fig. 10. The solid lines represent Monte Carlo simulations of Experiment #3 (irradiation at different temperatures), and are compared with selected experimental data from Fig. 3. MC was carried out with the same set of parameters as in Fig. 9. The value of the critical distance for the 4 RTL graphs shown here are $r'_c = 0,\ 0.7,\ 1.0,\ 1.28$.

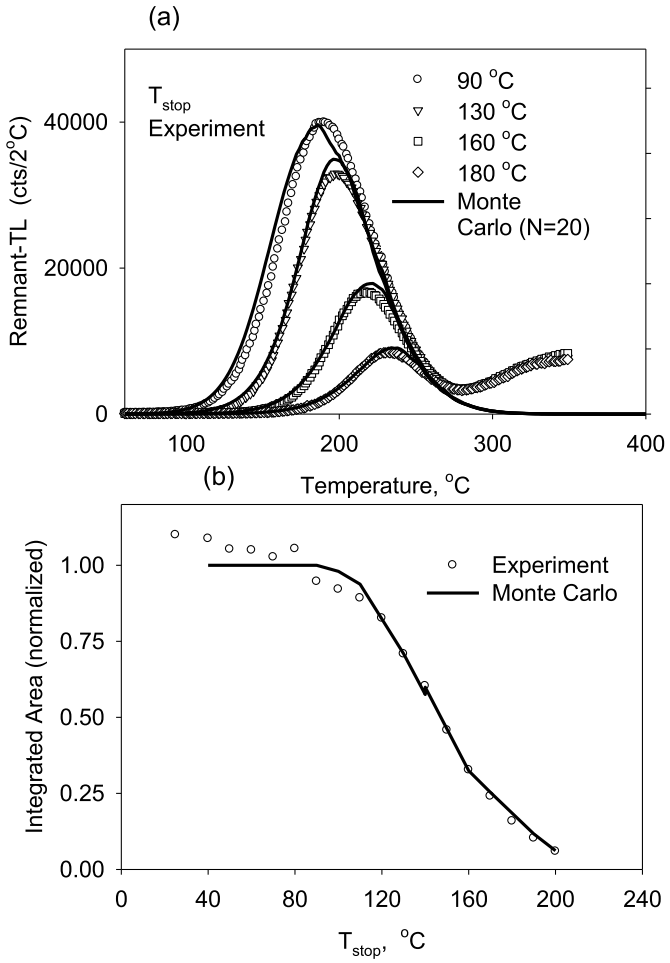

Fig. 11. The solid lines represent Monte Carlo simulations of Experiment #4 (preheating to T_{STOP}), and are compared with selected experimental data from Fig. 4. MC was carried out with the same set of parameters as in Figs. 9 and 10. The value of the critical distance for the 4 RTL graphs shown here are $r'_c = 0,\ 0.72,\ 1.06,\ 1.25$.

process for this subset of TL glow curves.

The MC simulations in Fig. 8 were carried out with the parameters: $E = 1.01$ eV, $A_{TL} = 2 \times 10^{11}$ s^{-1} and $\rho' = 0.019$. The values of the critical distance for the four MC simulations in Fig. 8 was taken as $r'_c = 0$, since the samples were not treated thermally after irradiation.

The MC simulations in Figs. 9–11 were carried out with the following slightly modified single set of parameters: $E = 1.02$ eV, $A_{TL} = 2 \times 10^{11}$ s^{-1} and $\rho' = 0.01$. The value of the critical distance for the MC simulations in Figs. 9–11 are indicated in the legend of these figures. The value of the kinetic parameter $\rho' = 0.01$ is in close agreement with the value obtained for several feldspars samples by Polymeris et al. [22].

Fig. 10b shows the variation of the integrated TL intensity from Fig. 3, as a function of the irradiation temperature T_{IRR}, for Experiment #3. As the irradiation temperature increases, the TL intensity decreases. The solid line indicates the results of the MC simulations; these compare very well with the experimental data, indicating that the thermal behavior of the sample at different irradiation temperatures is described in a satisfactory manner. Similarly, Fig. 10b shows the variation of the integrated TL intensity from Fig. 4, as a function of the temperature T_{STOP} for Experiment #4. As the temperature T_{STOP} increases, the TL intensity decreases. Once more, the MC simulations (solid line) agree with the experimental data, with some small deviations observed at lower temperatures T_{STOP}. These deviations are within the accuracy/precision limits of these experiments.

6. Discussion and conclusions

In this paper, four different types of experiments were described quantitatively with the MC method based on the single differential equations (1) and (8), for both unheated and preheated samples. Unheated samples are described with a critical radius value $r'_c = 0$, while for preheated samples the values of the critical radius r'_c are finite. Thermal treatment of the samples causes the TL glow peaks to appear shifted towards higher temperatures, while they maintain their symmetric shape and width. A detailed theoretical justification of the unchanging shape of TL glow peaks for pretreated samples is given in Pagonis and Brown ([21]).

The results of this paper show that the Monte Carlo method of Pagonis et al. [15] is an efficient simple method of fitting experimental TL glow peaks in MgB_4O_7, feldspars etc. This method has the added advantage that it is based on reasonable physical assumptions made within the model by Jain [18], for a random pair distribution of donors and acceptors interacting via tunneling processes.

The symmetric shape of the TL glow peaks in Experiments #1-#4 is consistent with the simulations of Kitis and Pagonis ([23,24]) based on the model by Jain et al. [18]. These authors showed that the width of the TL glow curve depends rather weakly on the kinetic parameters *E, s* and depends mostly on the concentration of acceptors ρ'. For typical experimental ρ' values in the range $\rho' = 0.005$-0.02, the model predicts very nearly symmetric TL glow peaks.

It is interesting to note that the unchanging shape of the TL glow peaks was also observed for a variety of feldspars which exhibit quantum tunneling phenomena including anomalous fading (Pagonis et al., [25]).

Another important result from the model results from comparing Fig. 7a and e. These two figures show that the behavior of irradiated samples in the laboratory may be very different from that of samples irradiated in nature, due to the much smaller natural irradiation rate. We interpret this behavior to mean that sites which can populate at high laboratory dose rates (and therefore high trapping rates) are unstable at low natural dose rates, despite the fact that the detrapping rates may be the same. However, despite changes in the position of the initial rise of the curve, the shape of the TL glow peaks again does not depend on the dose rate. This result is of importance for thermochronometry and temperature sensing applications; the unchanging shape of the TL glow peaks means that the temperature of maximum TL intensity (T_{MAX}) can be used to quantify the thermal history of the samples.

It is noted that similar series of TL glow curves have been reported for other types of dosimetric materials by several researchers. Such composite TL peaks were studied under different experimental conditions, and have been investigated for example in $Ca_5(PO_4)_3OH:Gd^{3+},Pr^{3+}$ by Mokoena et al. [27], and in $SrAl_2O_4:Eu^{2+},Dy^{3+}$ by Chithambo et al. ([28,29]). The experimental data in these studies have been interpreted on the basis of luminescence mechanisms different from the quantum tunneling processes used in this paper.

For additional recent discussions of the possibility of using doped MgB_4O_7 and other materials for thermochronometry and temperature sensing, the reader is referred to the work of Yukihara et al. [11], and Biswas et al. [26].

References

[1] S.W.S. McKeever, M. Moscovitch, P.D. Townsend, Thermoluminescence Dosimetry Materials: Properties and Uses, Nuclear Technology Publishing,Ashford, 1995.
[2] M. Prokic, Development of highly sensitive $CaSO_4$:Dy/Tm and MgB_4O7:Dy,Tm sintered thermoluminescent dosimeters, Nucl. Instrum. Methods 175 (1980) 83.
[3] M. Prokic, MgB_4O_7:Mn as a new TL dosemeter, Radiat. Protect. Dosim. 47 (1993) 191.
[4] M. Prokic, Individual monitoring based on magnesium borate, Radiat. Protect. Dosim. 125 (2007) 247.

[5] C.M.H. Driscoll, Sensitivity and fading characteristics of thermoluminescent magnesium borate, Radiat. Protect. Dosim. 1 (1981) 135.
[6] C. Furetta, M. Prokic, R. Salamon, G. Kitis, Dosimetric characterization of a new production MgB_4O_7:Dy,Na, Appl. Radiat. Isot. 52 (2000) 243–250.
[7] S.P. Lochab, A. Pandey, P.D. Sahare, R.S. Chauhan, N. Salah, R. Ranjan, Nanocrystalline MgB_4O_7:Dy for high dose measurement of gamma radiation, Phys. Status Solidi 204 (2007) 2416.
[8] J.L. Price, N.A. Guardala, G.K. Riel, V.K. Mathur, Neutron response of a laser heated thermoluminescence dosimetry system, Radiat. Meas. 29 (1998) 379.
[9] E.G. Yukihara, E.D. Milliken, B.A. Doull, Thermally stimulated and recombination processes in MgB_4O_7 investigated by systematic lanthanide doping, J. Lumin. 154 (2014) 251.
[10] E.G. Yukihara, A.C. Colleman, B. Doull, Passive temperature sensing using thermoluminescence: laboratory tests using Li_2B4O_7:Cu,Ag, $MgB4O_7$:Dy,Li and $CaSO_4$:Ce,Tb, J. Lumin. 146 (2014) 515.
[11] E.G. Yukihara, C. Coleman, R.H. Biswas, R. Lambert, F. Herman, G.E. King, Thermoluminescence analysis for particle temperature sensing and thermochronometry: principles and fundamental challenges, Radiat. Meas. 120 (2018) 274–280 2018.
[12] T. Karali, A.P. Rowlands, M. Prokic, P.D. Townsend, E. Halmagean, Thermoluminescent spectra of rare earth doped MgB_4O_7 dosemeters, Radiat. Protect. Dosim. 100 (2002) 191.
[13] G. Kitis, G.S. Polymeris, I.K. Sfampa, M. Prokic, N. Meriç, V. Pagonis, Prompt isothermal decay of thermoluminescence in MgB_4O_7:Dy, Na and LiB_4O_7:Cu, in dosimeters, Radiat. Meas. 84 (2016) 15–25.
[14] N. Brown, E.J. Rhodes, T. Harrison, Mark, Using thermoluminescence signals from feldspars for low-temperature thermochronology, Quat. Geochronol. 42 (2017) 31–41.
[15] V. Pagonis, J. Friedrich, M. Discher, A. Müller-Kirschbaum, V. Schlosser, S. Kreutzer, R. Chen, C. Schmidt, Excited state luminescence signals from a random distribution of defects: a new Monte Carlo simulation approach for feldspar, J. Lumin. 207 (2019) 266–272 March 2019.
[16] C. Furetta, M. Prokic, R. Salamon, G. Kitis, Dosimetric characterisation of a new production of MgB_4O_7:Dy,Na thermoluminescent material, Appl. Radiat. Isot. 52 (2000) 243–250.
[17] C. Furetta, G. Kitis, P.S. Weng, T.C. Chu, Thermoluminescence characteristics of MgB_4O_7:Dy,Na, Nucl. Instrum. Method Phys. Res. B 420 (1999) 441–445.
[18] M. Jain, B. Guralnik, M.T. Andersen, Stimulated luminescence emission from localized recombination in randomly distributed defects, J. Phys. Condens. Matter 24 (2012) 385402.
[19] V. Pagonis, P. Morthekai, G. Kitis, Kinetic analysis of thermoluminescence glow curves in feldspar: evidence of a continuous distribution of energies, Geochronometria 41 (2) (2014) 168–177.
[20] I.K. Sfampa, G.S. Polymeris, V. Pagonis, E. Theodosoglou, N.C. Tsirliganis, G. Kitis, Correlations of basic TL,OSL and IRSL properties of ten K-feldspar samples of various origin, Nucl. Instrum. Methods Phys. Res. B 359 (2015) 89–98.
[21] V. Pagonis, N. Brown, On the unchanging shape of thermoluminescence peaks in preheated feldspars: implications for temperature sensing and thermochronometry, Radiat. Meas. 124 (2019) 19–28.
[22] G.S. Polymeris, V. Pagonis, G. Kitis, Thermoluminescence glow curves in preheated feldspar samples: an interpretation based on random defect distributions, Radiat. Meas. 97 (2017) 20–27.
[23] G. Kitis, V. Pagonis, Analytical solutions for stimulated luminescence emission from tunneling recombination in random distribution of defects, J. Lumin. 137 (2013) 109–115.
[24] G. Kitis, V. Pagonis, Properties of thermoluminescence glow curves from tunneling recombinations processes in random distributions of defects, J. Lumin. 153 (2014) 118–124.
[25] V. Pagonis, F. Marques dos Santos Vieira, A. Chambers, L. Anthony, Thermoluminescence glow curves in preheated feldspars: a Monte Carlo study, Nucl. Instrum. Methods Phys. Res. B. 436 (2018) 249–256, https://doi.org/10.1016/j.nimb.2018.09.036 Available online as.
[26] R.H. Biswas, F. Herman, G.E. King, J. Braun, Thermoluminescence of feldspar as a multi-thermochronometer to constrain the temporal variation of rock exhumation in the recent past. Earth and Planetary Science Letters 495, (2018), https://doi.org/10.1016/j.epsl.2018.04.030 Available online at.
[27] P.P. Mokoena, M.L. Chithambo, Vinay Kumar, H.C. Swart, H.C, O.M. Ntwaeaborwa, Thermoluminescence of calcium phosphate co-doped with gadolinium and praseodymium, Radiat. Meas. 77 (2015) 26–33.
[28] M.L. Chithambo, Thermoluminescence of the main peak in $SrAl_2O_4$:Eu^{2+}, Dy^{3+}: spectral and kinetics features of secondary emission detected in the ultra-violet region, Radiat. Meas. 96 (2017) 29–41.
[29] M.L. Chithambo, A.H. Wako, A.A. Finch, Thermoluminescence of $SrAl_2O_4$:Eu^{2+}, Dy^{3+}: kinetic analysis of a composite-peak, Radiat. Meas. 97 (2017) 1–13.